Int. J. Heat Mass Transfer. Vol. 29, No. 7, pp. 987–997, 1986
Printed in Great Britain

0017–9310/86 $3.00 + 0.00
Pergamon Journals Ltd.

Effect of interwall spacing on heat transfer and pressure drop in a corrugated-wall duct

M. MOLKI* and C. M. YUEN
Department of Mechanical Engineering, Tufts University, Medford, MA 02155, U.S.A.

(*Received* 28 *May* 1985 *and in final form* 23 *December* 1985)

Abstract—Experiments were conducted to determine the axial distribution of per-facet and per-cycle heat transfer coefficients for turbulent flow in an isothermal, corrugated-wall duct with variable interwall spacing. The investigation was conducted via a mass transfer technique. The focus of the study was on two regions of the duct: the combined thermal–hydraulic entrance region and the periodic, fully developed region. A visualization technique was employed to examine the effect of interwall spacing on the pattern of fluid flow. Pressure drop and heat transfer results were employed to evaluate the thermal performance of the duct.

INTRODUCTION

AN EXPERIMENTAL investigation was conducted to study convective heat transfer in an isothermal, corrugated-wall duct with variable interwall spacing. The work was concentrated on two regions: the entrance region where the velocity and temperature profiles changed simultaneously, and the fully developed region.

Corrugated ducts have been employed in a number of engineering devices to enhance heat transfer and to achieve higher thermal performance. They have been successfully used in compact heat exchangers, resulting in a more economical use of space and material. The problem of internal heat generation in modern high-speed computers, which has recently become a serious limiting factor in their design, has been solved in certain computers by incorporating corrugated-wall channels into their cooling system. Heat transfer in gas turbines, which is often enhanced by turbulence promoters and jet impingement, may also be improved by installing corrugations in their internal cooling passages with an optimum spacing. All these applications involve relatively short flow passages in which fully developed conditions are not likely to exist; however, when they do exist, the entrance effect on the overall transfer coefficient is expected to be significant. In the case of turbine blades, several cooling passages usually run along the radial length of the blade with different aspect ratios and, in addition to the entrance effect, the effect of aspect ratio (or interwall spacing) on heat transfer seems to be important.

A search of the literature reveals only a limited number of publications related to the present problem. Goldstein and Sparrow [1] conducted experiments to determine local transfer characteristics for flow in a relatively short, corrugated-wall channel. In another work [2], the same authors examined a corrugated fin-and-tube heat exchanger configuration and determined the local and average transfer coefficients via a mass transfer technique.

O'Brien and Sparrow [3] employed the conventional method of resistance (ohmic) heating to study turbulent heat transfer in a corrugated duct with fixed spacing and corrugation angle. Although temperature measurements at the wall were reported for the entrance region, the main focus of their work was on the developed section of the duct. The experimental apparatus of ref. [3] was later modified to study heat transfer with a larger interwall spacing and different inlet configurations [4].

In the present investigation, we did not use the conventional direct method of resistance heating; instead, a mass transfer technique known as naphthalene sublimation was employed to increase the accuracy of the results and to give better control over the thermal boundary conditions. This technique completely eliminated the axial component of heat conduction and enabled us to examine the effect of interwall spacing on the transfer characteristics of the entrance region. Mass transfer results were subsequently converted to heat transfer results by application of the analogy between the two processes.

The test duct had only two corrugated walls—the upper and the lower walls—and the corrugations were fabricated from solid naphthalene. The side walls were smooth and free from naphthalene and, therefore, they did not participate in the mass transfer process. This arrangement made it possible to study the effect of corrugations on enhancement of transfer coefficients without the thermal interference of the side walls.

With regard to the boundary conditions, the present problem is quite different from those reported in the literature [3, 4]. The mass transfer model considered here is analogous to a heat transfer problem in which

* Present Address: Department of Mechanical Engineering, Esfahan University of Technology, Esfahan, Iran.

NOMENCLATURE

A_i	mass transfer area per module	Sc	Schmidt number
D_h	hydraulic diameter of the duct	Sh_{fd}	fully developed Sherwood number
$\mathscr{D}$	diffusion coefficient	$\overline{Sh}_{fd}$	cycle average, fully developed Sherwood number
f	friction factor	$\overline{Sh}^*_{fd}$	modified Sherwood number
H	perpendicular spacing between corrugated walls	Sh_{smooth}	Sherwood number for straight duct with smooth walls
h	convective heat transfer coefficient	V	mean fluid velocity
K_i	mass transfer coefficient for module i	X	axial coordinate
L	axial length of a corrugation cycle	W	duct width
$\dot{M}_i$	per-module rate of mass sublimation		
$\overline{Nu}_{fd}$	cycle average fully developed Nusselt number	Greek symbols	
Nu_{smooth}	Nusselt number for straight duct with smooth walls	ν	kinematic viscosity
P	air pressure; perimeter of the duct, $2(H+W)$	ρ	density
Pr	Prandtl number	ρ_{nb}	naphthalene vapor density in bulk
$\dot{Q}_i$	volumetric air flow rate at the axial location of module i	ρ_{nw}	naphthalene vapor density at wall
Re	Reynolds number	$\Delta\rho_{n,i}$	wall-to-bulk difference in naphthalene vapor density for module i, $(\rho_{nw}-\rho_{nb})_i$
		θ	corrugation angle, 30°.

the corrugated walls are ideally isothermal and the side walls are adiabatic.

With these thermal conditions, two types of transfer coefficients were investigated: one was the per-facet coefficient, and the other was the average coefficient for a whole corrugation. The interwall spacing ranged from 0.476 to 0.953 cm with Reynolds number between 4000 and 35,000.

The mass transfer experiments were complemented with flow visualization and pressure measurements. The pressure results were then used to determine the optimum interwall spacing for the best thermal–hydraulic performance of the duct.

THE EXPERIMENTAL APPARATUS AND PROCEDURE

The description of the apparatus is facilitated by reference to Fig. 1 where various components of the apparatus—the test section, plenum chamber, rotameter, control valve and blower—are shown schematically. The test section, which is considered to be the heart of the apparatus, was a corrugated duct with naphthalene-coated corrugations where the mass transfer occurred. The blower operated in the suction mode to draw the laboratory air into the apparatus and to discharge the naphthalene-laden exhaust air to

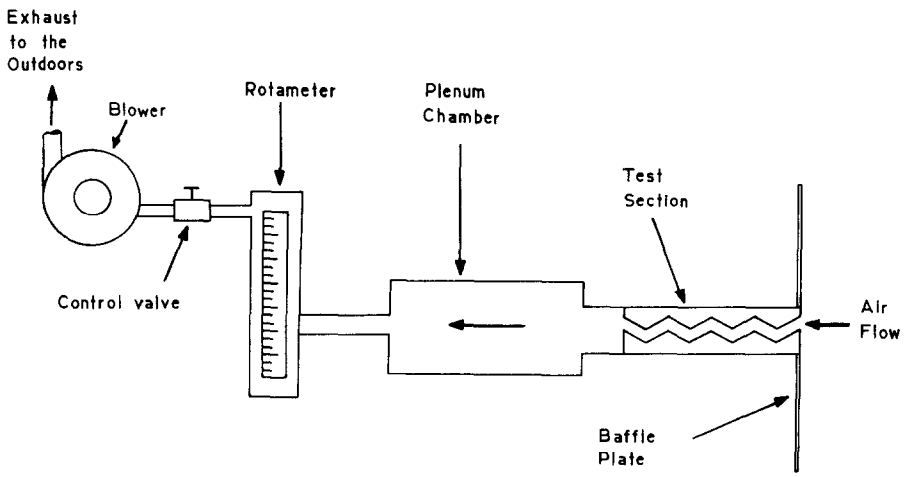

FIG. 1. The experimental apparatus.

the outdoors. This flow arrangement ensured that the laboratory would remain free from naphthalene vapor and that the heat generated by the blower would not interfere with the constancy of the inlet air temperature during an experimental run. The rotameter shown in Fig. 1 is designed for airflow mesurements and is pre-calibrated by the manufacturer. The desired mass flow rate was established by a combination of partially closing the control valve and varying the input voltage of the blower by means of a Variac. The major role of the partially closed valve was to damp out the undesirable flow fluctuations and to provide a steady flow of air throughout the flow circuit.

The test section was assembled from a number of modules, and a typical assembly where each module is flanked by the adjacent upstream and downstream modules, is pictured in Fig. 2. As shown, each module consists of a metallic base and a tapered layer of solid naphthalene formed by a casting process. The metallic base was an aluminium segment whose upstream- and downstream-facing facets were machined to yield a very smooth surface to ensure that the contact between the neighboring modules was ideal.

The duct components were assembled in such a way that the axial location of the peaks of corrugations on one wall coincided with the axial location of the valleys on the other wall. The sides of the duct were covered by two smooth side walls (not shown) which maintained the spacing H between the opposite facets of corrugations. The spacing H was a significant factor in the present investigation and was varied systematically by changing the side walls. The angle of corrugation was 30°, and the width of the duct W was constant and equal to 3.81 cm.

As many as 40 modules were assembled to form the corrugated duct. The entire assembly of modules was then placed in a support housing with pressure-sensitive tape and rubber gaskets used to seal the joints against leaks.

During the data run, the naphthalene surface temperature was recorded several times by a Kaye data logger with a resolution of 0.1°F. The vapor pressure and other properties were then evaluated at the arithmetic mean of the recorded temperatures. The modules were individually weighed on a Sartorius 2432 balance and the mass changes were determined to within 0.1 mg.

A separate test section was constructed for measurements of axial pressure drop. The upper and lower walls of this test section were fabricated entirely from aluminum and had the same surface geometry as that of the mass transfer experiments. At a given flow rate, the pressure signals from the taps were conveyed through plastic tubing to a Baratron pressure transducer and recorded on a Fluke 2200B data logger.

FLOW VISUALIZATION

The test section for pressure measurements was also used in the flow visualization experiments. The flow visualization was performed by the oil–lampblack technique. As a first step, the small pressure taps on the upper corrugated wall were carefully covered with tape. To facilitate the use of this technique, the corrugations of the lower wall were covered with white contact paper. Before the airflow was activated, the contact paper was brushed with a suitable mixture of oil and lampblack, and the test section was assembled to form a corrugated flow passage with a given H. Then, the airflow was activated and the development of the flow patterns was visually observed through the Plexiglass side walls of the duct. It should be noted that prior to the activation of the airflow, the black

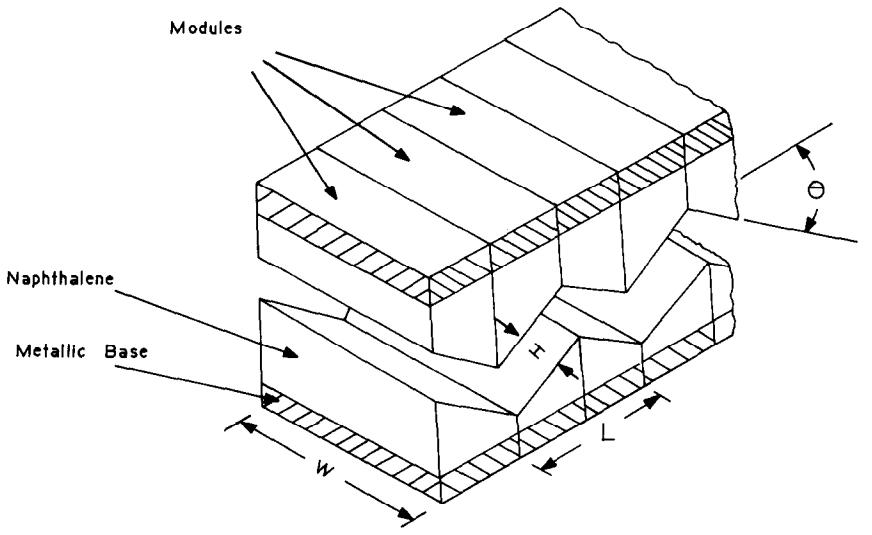

FIG. 2. Perspective view of the corrugated duct.

coating on the facets of corrugations appeared as a smooth, glossy-black surface. However, with the visualization run in progress, the airflow exerted a shearing force on the black mixture and moved it along the surface, following the path of the fluid particles that passed adjacent to the surfacre. At the end of a flow visualization run, the black streaks that appeared on the white background of the contact paper revealed the pattern of fluid flow adjacent to the facets and the neighborhood of the corrugations. The information conveyed by these patterns and those revealed through the direct visual observation of the flow during the run were used to prepare a number of sketches to be presented shortly.

The schematic of the visualized flow patterns, prepared for the periodically fully developed region of the duct and shown by their respective side views, are presented in Fig. 3. The Reynolds number for flow visualization runs was 30,000.

An overall examination of the figure reveals a common flow pattern among the three cases, namely, the existence of a separated flow with a recirculation zone. However, the major difference between these three cases is in the size of the separation bubble and the location of the point of reattachment. As seen in the figure, in the case of the smallest spacing (i.e. $H/L = 0.25$), the separation bubble is relatively small and the recirculation zone is limited to the immediate downstream of the corrugation peak and to the downstream-facing facet of the corrugation. For the other two cases where the spacing H/L is increased to 0.363 and then to 0.50, the separation bubble consistently expanded to shroud a portion of the neighboring upstream-facing facet. Moreover, the point of flow reattachment moved farther downstream and is on the upstream-facing facet of the next corrugation. These qualitative results are consistent with the observations of other investigators [3, 4].

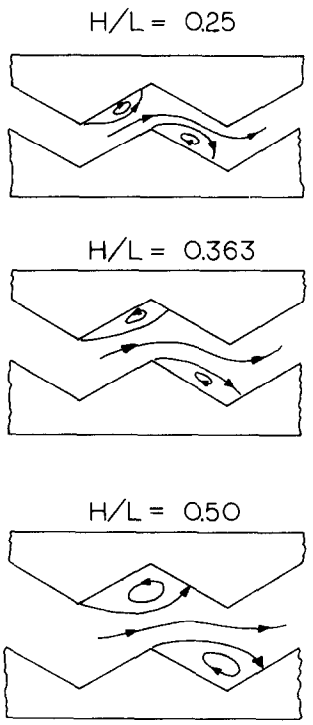

FIG. 3. Patterns of fluid flow.

The flow visualization results, as discussed above, indicate that the patterns of fluid flow are significantly affected by the interwall spacing of the duct. With regard to the forthcoming mass transfer results, perhaps the most important finding of the flow visualization is that for a specified Reynolds number, the increased interwall spacing consistently shifts the point of reattachment downstream and enlarges the separated flow region.

MASS (HEAT) TRANSFER RESULTS

Data reduction

The mass transfer coefficient for a typical module i was evaluated from its conventional defining equation

$$K_i = \dot{M}_i / A_i \Delta\rho_{n,i}. \tag{1}$$

In this equation, $\dot{M}_i$ is the per-module rate of mass sublimation and was determined from the amount of mass sublimated from module i during the run time, A_i is the mass transfer surface area, and $\Delta\rho_{n,i}$ is the wall-to-bulk difference in naphthalene vapor density at the axial mid-point of the module.

The evaluation of $\Delta\rho_n$ requires knowledge of the axial variation of the bulk vapor density of naphthalene in the air stream (ρ_{nb}) and the naphthalene vapor density at the wall (ρ_{nw}). To determine ρ_{nw}, the naphthalene vapor pressure at the wall was evaluated from Sogin's vapor pressure–temperature correlation [5] and then substituted into the ideal gas equation. It should be noted that the test section was isothermal and that ρ_{nw} was the same for all modules.

To find ρ_{nb} at the axial mid-point of a module, the following expressions were developed from a mass balance performed on a control volume that encompassed the portion of the duct from the inlet up to the axial mid-point of the ith module ($i > 3$)

$$\rho_{nb,i} = (\dot{M}_1 + 2\sum_{j=2}^{i-2} \dot{M}_j + 2.5\dot{M}_{(i-1)} + 1.5\dot{M}_i)/\dot{Q}_i. \tag{2}$$

In a similar manner, for the first, second, and third modules we have

$$\rho_{nb,1} = 0.5(\dot{M}_1 + \dot{M}_2)/\dot{Q}_1 \tag{3}$$

$$\rho_{nb,2} = 1.5(\dot{M}_1 + \dot{M}_2)/\dot{Q}_2 \tag{4}$$

$$\rho_{nb,3} = (\dot{M}_1 + 2.5\dot{M}_2 + 1.5\dot{M}_3)/\dot{Q}_3. \tag{5}$$

In equations (2)–(5), $\dot{M}_i$ and $\dot{Q}_i$ represent the rate of mass sublimation and volumetric air flow rate corresponding to module i.

Next, the mass transfer coefficients evaluated from equation (1) are nondimensionalized through the

definition of Sherwood number and presented for the ith module as

$$Sh_i = K_i D_h / \mathscr{D} \tag{6}$$

where $\mathscr{D}$ is the diffusion coefficient, and D_h is the hydraulic diameter of the duct defined as

$$D_h = 4A/P \tag{7}$$

in which $A = HW$ and $P = 2(H+W)$.

The diffusion coefficient $\mathscr{D}$ was determined from the definition of Schmidt number $Sc = \nu/\mathscr{D}$. For naphthalene diffusion in air, $Sc = 2.5$ [5]. Due to small concentrations of naphthalene vapor, the kinematic viscosity ν was taken as that for pure air.

The mass transfer results will be presented in terms of the duct Reynolds number Re, defined based on the hydraulic diameter as

$$Re = VD_h/\nu \tag{8}$$

where V is the mean fluid velocity across the minimum flow area A.

Fully developed transfer coefficients

The present experimental work employed a mass transfer technique whose reliability and precision has been indicated by a number of reports in the published literature. To provide additional support for this technique, it was decided—as a first step—to investigate the transfer characteristics of a smooth straight duct and to make a comparison with literature.

The fully developed Sherwood numbers as a function of Reynolds number are presented in Fig. 4 for the smooth duct. The aspect ratio of the smooth duct was 8:1, which corresponds to $H/L = 0.25$. Also shown in this figure are the well-known Petukhov–Popov correlation [6], the modified version of that correlation by Gnielinski [7], and the equation obtained by Sparrow and Cur [8]. The close agreement

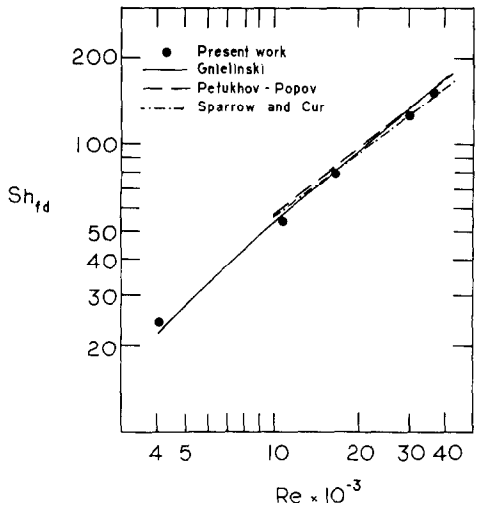

FIG. 4. Fully developed Sherwood number for the smooth duct.

seen between the data points of this investigation and literature is well supportive of the present experimental approach.

Attention is now turned to the transfer coefficients of the corrugated duct which is the main objective of the present investigation. The periodic, fully developed Sherwood number for the upstream- and downstream-facing facets are presented in Fig. 5 using H/L as a parameter. Three values of H/L were employed, namely, 0.25, 0.363 and 0.50. The solid lines passing through the data are the least-squares fits. The equations for the upstream-facing facets are

$$Sh_{fd} = 0.288Re^{0.670}, \quad (H/L = 0.25) \tag{9}$$

$$= 0.355Re^{0.680}, \quad (H/L = 0.363) \tag{10}$$

$$= 0.265Re^{0.736}, \quad (H/L = 0.50) \tag{11}$$

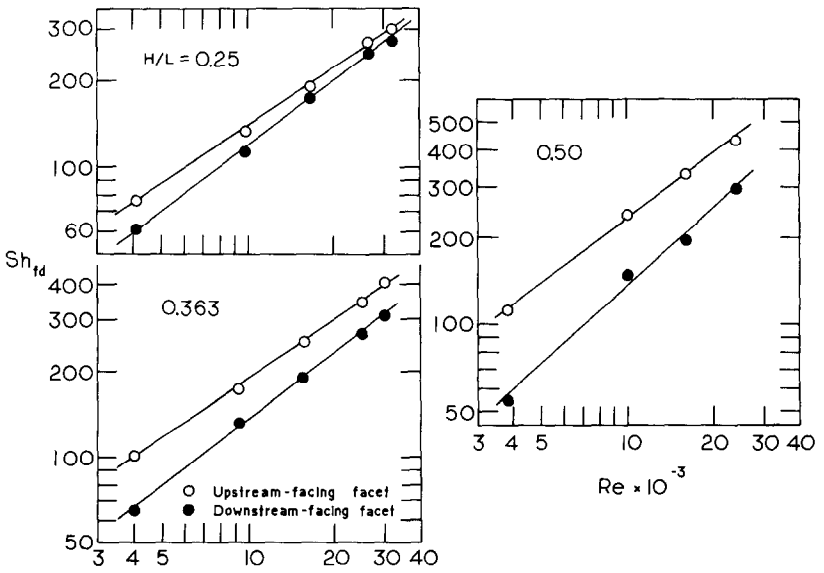

FIG. 5. Periodic, fully developed Sherwood number for individual facets of corrugation.

and those for the downstream-facing facets are

$$Sh_{fd} = 0.118Re^{0.749}, \quad (H/L = 0.25) \qquad (12)$$

$$= 0.118Re^{0.765}, \quad (H/L = 0.363) \qquad (13)$$

$$= 0.034Re^{0.899}, \quad (H/L = 0.50). \qquad (14)$$

Equations (9)–(14) indicate that the Sh_{fd} for the downstream-facing facets is more responsive to Reynolds number than that for the upstream-facing facet. This trend is quite expected and is in agreement with the literature information that the transfer coefficients for the separated flows show higher Reynolds number dependency as compared to the unseparated flows. Furthermore the exponent 2/3, which well approximates the exponents 0.670, 0.680, and to some extent, 0.736 of the equations (9)–(11), has been encountered in a number of physical situations involving turbulent separated and reattached flows [9, 10, 11].

Inspection of the data for the upstream-facing facet in Fig. 5 shows that the per-facet Sherwood numbers for $H/L = 0.50$ are largest, while those corresponding to $H/L = 0.363$ and 0.25 are, respectively, the intermediate and the smallest at a given Reynolds number. Thus, it appears that an increase of the interwall spacing has a favorable effect on the mass transfer from the facet. However, the Sherwood number, as defined in equation (6), not only reflects the variations of the mass transfer coefficient, but also reveals the effect of the hydraulic diameter of the duct. If variations of the hydraulic diameter are also taken into account, the data points show that as the interwall spacing is increased the per-facet mass transfer coefficients are decreased. In the range of Re considered in this investigation, the maximum reduction in the mass transfer coefficient when H/L was increased first from 0.25 to 0.363 and, then, to 0.50, was reduced by 3.7% and 13.4%, respectively. These maximum percentages corresponded to $Re = 4000$.

Finally, the data for downstream-facing facets in Fig. 5 show that as H/L is increased the Sherwood numbers change only slightly. However, considering the variations in the hydraulic diameter as H/L varied from 0.25 to 0.363, and then to 0.50, the mass transfer coefficients experienced the maximum reduction of 21.7% and 78.7%, respectively.

The periodic, fully developed Sherwood numbers—averaged over a cycle of corrugation—are presented in Fig. 6. The data for the $H/L = 0.25$, 0.363 and 0.50 interwall spacings in the fully turbulent region ($Re > 10{,}000$) have been fitted with least-squares straight lines, yielding the following equations

$$\overline{Sh}_{fd} = 0.159Re^{0.724}, \quad (H/L = 0.25) \qquad (15)$$

$$= 0.213Re^{0.719}, \quad (H/L = 0.363) \qquad (16)$$

$$= 0.261Re^{0.717}, \quad (H/L = 0.50). \qquad (17)$$

Also shown in Fig. 6 are the heat transfer results reported by Beloborodov and Volgin [12] and O'Brien and Sparrow [3], which have been converted to mass

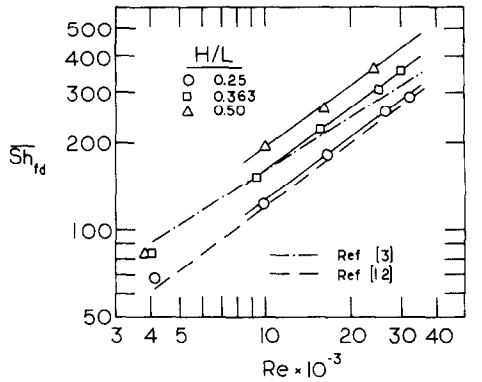

FIG. 6. Cycle average, periodic, fully developed Sherwood number.

transfer at $Pr = 2.5$ (or $Sc = 2.5$) via the analogy between the two processes. As seen, the level of agreement between ref. [12] and the data points of the present investigation for $H/L = 0.25$ is very good. However, there are some differences between the heat transfer predictions of ref. [3], which were obtained for $H/L = 0.25$, and the corresponding mass transfer data of the present work. The differences, ranging from 34% at $Re = 4000$ to 14% at $Re = 32{,}000$, are not surprising, considering the many differences between the two experiments.

With a view to bringing together the data for the $H/L = 0.25$, 0.363 and 0.50 cases in the range of Re corresponding to the fully turbulent region, an additional curve-fitting procedure suggested a modified Sherwood number $\overline{Sh}^*_{fd}$ defined as

$$\overline{Sh}^*_{fd} = -\ln \overline{Sh}_{fd} + (\ln Re) \exp 0.005/(H/L) - 0.343. \qquad (18)$$

A graph of $\overline{Sh}^*_{fd}$ vs H/L (see Fig. 7) indicates that the dependence on Re has been successfully eliminated. The solid straight line in this figure is the least-squares fit to the data points with the equation

$$\ln \overline{Sh}^*_{fd} = -1.244(H/L) + 0.908. \qquad (19)$$

The modified Sherwood number in equation (19) conveys the information that is also implied by equations (15)–(17).

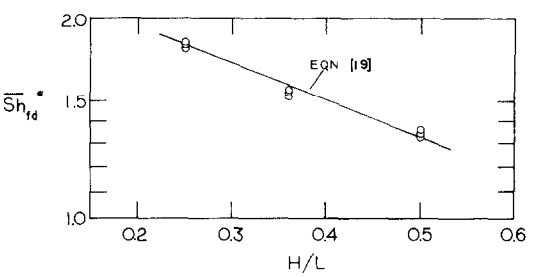

FIG. 7. Modified Sherwood number.

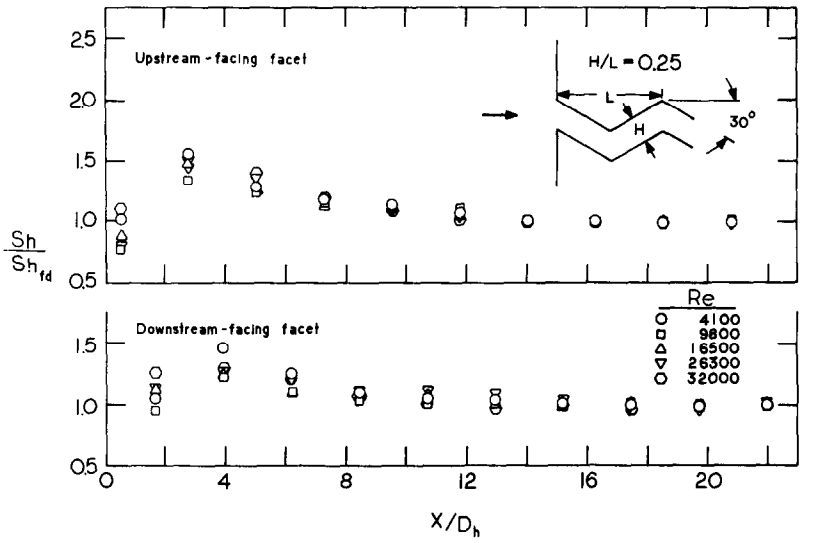

FIG. 8. Distribution of per-facet Sherwood number for the corrugated duct ($H/L = 0.25$).

Transfer coefficients in the entrance region

The per-facet Sherwood number in the entrance region of the corrugated duct are presented in Figs. 8–10. Each figure shows two sets of data. The upper set represents the transfer coefficients of the upstream-facing facets and the lower set represents those of the downstream-facing facets.

An overall review of the upper results indicate a trend that is to some extent similar to the distribution of transfer coefficients in the entrance region of a straight (smooth) data as reported in ref. [8]. Beginning with a relatively small value, Sh/Sh_{fd} increases rapidly to a maximum value at which point they start to decrease gradually along the axis of the duct and approach the fully developed value.

It is noteworthy that the variations of transfer coefficients in the entrance region of a straight duct are generally much larger than those observed in a corrugated duct (for example see ref. [8, Figs. 3–6]). On one hand when fluid enters a straight duct with a sharp-edged inlet, it experiences separation in the vicinity of the inlet which results in rapid variations of the transfer coefficients in this region. On the other hand in a corrugated duct, the flow is repeatedly separated downstream of each corrugation and the transfer coefficients are much higher than those in the straight duct.

Aside from the first set of data points, the results of the present investigation indicate that the transfer coefficients in the entrance region of the corrugated duct are consistently higher than those in the periodic, fully developed region. This was an anticipated outcome, since in the entrance region the concentration gradient of the mass transfer species at the wall is larger, resulting in higher coefficients.

The entry region transfer coefficients for the downstream-facing facets are presented in the lower portion of Figs. 8–10. Except for the results at the large Reyn-

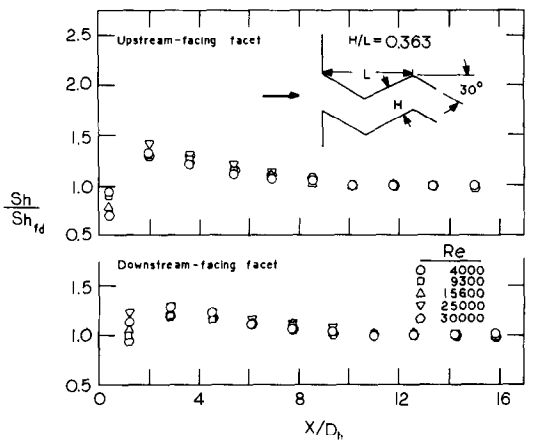

FIG. 9. Distribution of per-facet Sherwood number for the corrugated duct ($H/L = 0.363$).

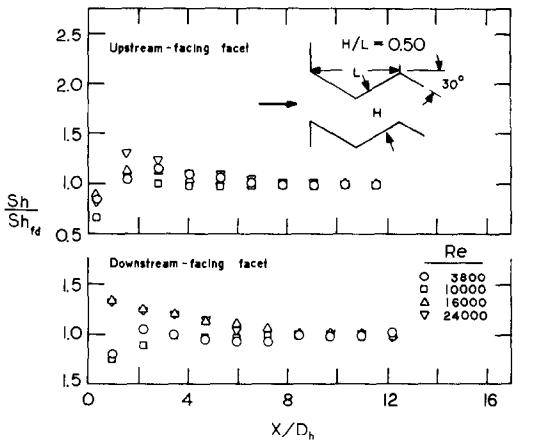

FIG. 10. Distribution of per-facet Sherwood number for the corrugated duct ($H/L = 0.50$).

olds numbers of $Re = 16{,}000$ and 24,000 and $H/L = 0.50$ (Fig. 10), the trend is similar to that already discussed for the upstream-facing facets, but with less enhancement in the entrance region. It appears that in this region mass transfer at the downstream-facing facets is basically determined by the nature of the flow (i.e. flow separation) rather than large concentration gradients that exist near the entrance.

EVALUATION OF THERMAL HYDRAULIC PERFORMANCE

Friction factors were calculated from

$$f = -(\mathrm{d}p/\mathrm{d}x)D_h/\tfrac{1}{2}\rho V^2 \qquad (20)$$

where V is the mean fluid velocity based on the cross-sectional surface area HW. The friction factors for the straight duct with $H/L = 0.25$ are compared with the modified Blasius equation [13] in Fig. 11. As seen, the results of the present investigation are well supported by the predictions of Blasius.

Next, the pressure measurements were carried out to determine the friction factor of the corrugated duct for three interwall spacings $H/L = 0.25$, 0.363 and 0.50. The friction factors are shown in Fig. 11. The solid lines represent the least-squares fit to the data points. From the figure, it is seen that the parameter H/L has an increasing effect on f. This observation, however, should be interpreted with great caution since the definition of friction factor as given by equation (20) involves the hydraulic diameter D_h which was varied three times in the course of pressure measurement experiments. Therefore, the large numerical values of f are more indicative of the increased D_h and, in fact, the recorded pressure drops per unit length were smaller for larger interwall spacings.

Further inspection of the figure indicates that friction factor f depends on Reynolds number and that the nature of this dependence is affected by H/L. At the smallest spacing $H/L = 0.25$, f appears to decrease linearly (on a log–log scale) with Re, a reminder that there might be a similarity between the mechanisms responsible for the pressure losses in this case and those in the case of straight duct. For larger spacings $H/L = 0.363$ and 0.50, f increases with Re, revealing a different trend.

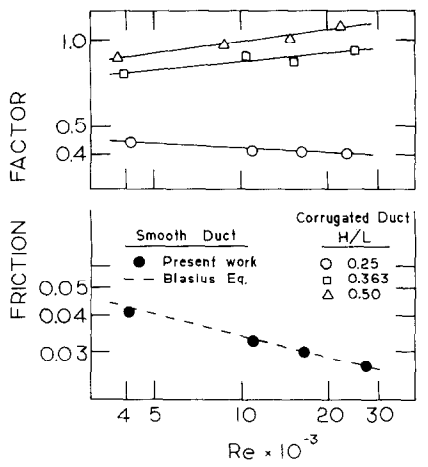

FIG. 11. Friction factor for smooth and corrugated ducts.

The flow visualization results discussed earlier may now be employed to interpret these changes in the shape of f–Re distributions. It is speculated that the pressure losses are governed by two components of drag—viscous and form drag—and that the relative importance of each component determines the trend of f distribution. On one hand for large H/L, the separated region expands and fills a major portion of the valley between neighboring corrugations, as a result of which the form drag becomes the dominant component. On the other hand due to enlarged spacing at a fixed Re, the contact surface area to volume ratio of the fluid decreases so that the overall effect is one of reducing the pressure drop per unit length of the duct. For $H/L = 0.363$ and 0.50, the dominating role of form drag on pressure losses is clearly seen from the direction of f dependence on Re in Fig. 11. When the interwall spacing is reduced to $H/L = 0.25$, the recirculating fluid occupies a smaller space and the viscous forces (skin friction) become the principal cause of pressure drop.

With friction factor and heat (mass) transfer results at hand, we can now examine the thermal performance of the corrugated duct for three different constraints: (a) identical pressure drop per unit length; (b) identical pumping power; and (c) identical mass flow. These constraints can be used to make two types of performance evaluation: one is to compare the Sherwood (or Nusselt) numbers of the corrugated duct to that of a straight duct with the same H/L for each of the aforementioned constraints; the other is to select one of the three corrugated ducts as a reference and compare the transfer coefficients of the other ducts (which have a different H/L) with that of the reference duct.

Attention is first turned to Fig. 12 where $\overline{Sh}_{fd}/Sh_{smooth}$, i.e. the periodic, fully developed Sherwood number of the corrugated duct (Fig. 6) divided by the Sherwood number of the smooth (straight) duct for one of the constraints (a)–(c), is presented as a function of Reynolds number.

From the defining equations for f, Re and the pumping power, it can be shown that

$$fRe^2 = (fRe^2)_{smooth} \quad \text{for identical pressure drop per unit length} \qquad (21)$$

$$fRe^3 = (fRe^3)_{smooth} \quad \text{for identical pumping power} \qquad (22)$$

$$Re = Re_{smooth} \quad \text{for identical mass flow.} \qquad (23)$$

The variables that appear on the left side in the above equations refer to the corrugated duct and those on

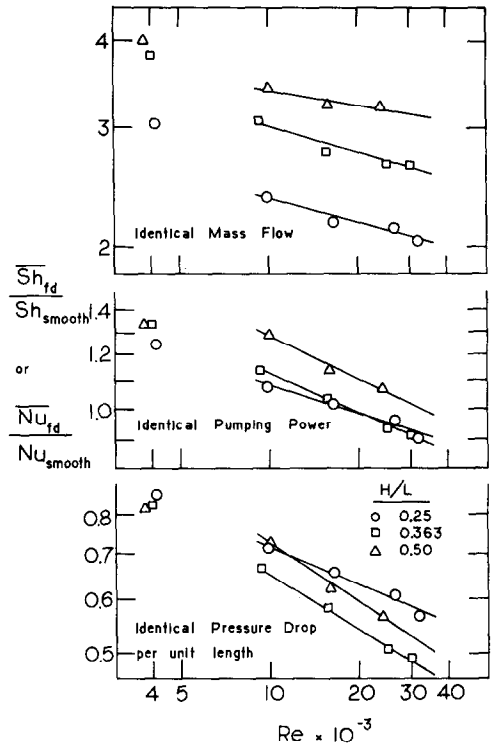

FIG. 12. The effect of H/L on thermal performance.

the right side with the subscript (smooth) apply to the smooth duct.

Examination of the lower diagram of Fig. 12 reveals that for a fixed pressure drop per unit length dp/dx and for the range of Re considered, the thermal performance of the corrugated ducts is worse than that of the straight duct. The situation becomes even more severe at higher Reynolds numbers. However, for the other two constraints namely, the identical pumping power and mass flow, the outcome of this investigation reveals an enhancement of the transfer coefficients except for very large Re of the latter constraint.

With identical pumping power at $Re = 4000$, the presence of corrugations in a duct improves the transfer coefficients by about 30%, and apparently with little dependence on the interwall spacing H/L. For higher values of Re, it appears that the performance of the duct depends on H/L and that the best performance is achieved when the duct has the largest interwall spacing. Nonetheless, when Re exceeds a certain value (e.g. $Re = 20{,}000$ for $H/L = 0.25$ and 0.363 and $Re = 34{,}000$ for $H/L = 0.50$), enhancement is no longer observed. The case of identical mass flow, shown in the top diagram of Fig. 12 is by far the most thermally efficient case which, under certain conditions, can improve heat transfer by up to about 400%.

The previous discussion enables the design engineer to decide whether it is advantageous to have a corrugated duct rather than a straight one. The next task, after deciding to have a corrugated duct, is to examine the effect of the interwall spacing on heat transfer coefficient under three constraints (a)–(c), and then to choose the spacing that yields the optimum thermal–hydraulic performance. In this connection, Fig. 13 is prepared where the ratio of heat transfer coefficients, h, for two corrugate ducts of different spacing is plotted in terms of Reynolds number. The subscripts 1, 2 and 3 refer, respectively, to the corrugated ducts with $H/L = 0.25$, 0.363 and 0.50. The abscissa Re_1 is the Reynolds number of the corrugated duct with $H/L = 0.25$.

As seen in the lower diagram of Fig. 13, the best thermal performance with identical pressure drop per unit length is achieved when the interwall spacing is the largest (i.e. $H/L = 0.50$). However, if the attainment of better thermal performance is the main objective, according to the lower diagram of Fig. 12 there is no need to employ a corrugated duct. Under the identical dp/dx constraint, the straight duct performs more efficiently, particularly at higher Reynolds numbers.

The middle diagram of Fig. 13 recommends either $H/L = 0.25$ or 0.50 as the most efficient configurations depending on the Reynolds number. The diagram at the top of this figure reveals that when the interwall spacing is systemically increased, the transfer coefficients decrease consistently, resulting in variation as high as 27%.

The results of the present investigation are compared with those reported by Sparrow and Comb [4] (Fig. 13) who conducted their experiments on a corrugated duct with $H/L = 0.363$ and compared their results with a previous work [3] where H/L was

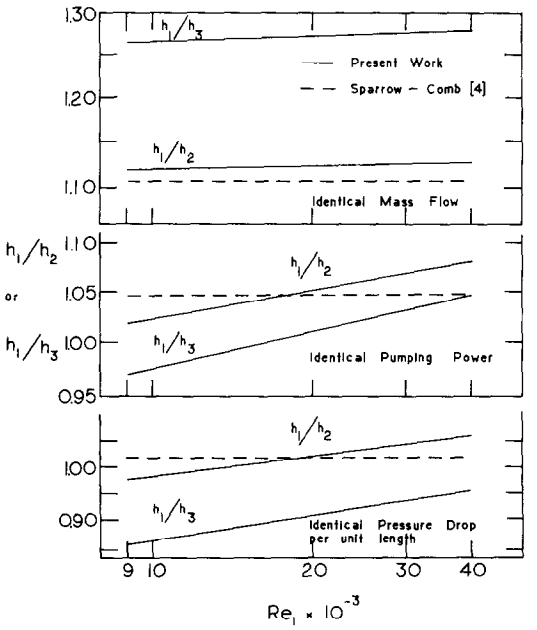

FIG. 13. The effect of interwall spacing on heat transfer coefficient.

0.25. Thus, the work of Sparrow and Comb—which is shown by the horizontal dashed lines—corresponds to the solid lines identified by h_1/h_2. In contrast to the present investigation which retained the Re dependency of f and $\overline{Sh}_{fd}$ in its entire calculations, ref. [4] employed the averaged friction factors and arrived at fixed numerical values for h_1/h_2. Nonetheless, the level of agreement seen in Fig. 13 is surprisingly good.

CONCLUDING REMARKS

The present investigation appears to be the first application of the naphthalene sublimation technique which addressed heat transfer simultaneously in the entrance region and the periodic, fully developed region of a corrugated duct under the variable interwall spacing condition. This technique successfully eliminated the losses that are normally associated with the heated components in a typical heat transfer experiment. However, it provided a well-defined boundary condition corresponding to that of the analogous heat transfer problem where the corrugated walls are isothermal and the side walls are adiabatic.

The visualization of the flow field indicated the significant effect of the interwall spacing on the patterns of fluid flow in the duct. It was shown that the flow separated just downstream of the corrugation peaks and reattached to the wall further downstream. The reattachment occurred either on the upstream-facing facet or on the downstream-facing facet, depending on the size of the interwall spacing.

The distribution of per-facet transfer coefficients indicated that the magnitude of these coefficients for the upstream- and downstream-facing facets are different with the difference decreasing with Reynolds number. For both facets, the Reynolds number dependency was reminiscent of the transfer characteristics of separated and reattached flows, which is consistent with the observed patterns of fluid flow. Moreover, inspection of the data revealed, taking the variations of the hydraulic diameter into account, that the dimensional transfer coefficients for the upstream- and downstream-facing facets both decreased with increasing interwall spacing. The maximum reduction with respect to the duct with the smallest spacing ranged from 3.7% to 13.4% for the first facet and 21.7% to 78.7% for the latter facet.

The effect of interwall spacing on per-facet Sherwood number was examined in the combined thermal–hydraulic entrance region of the duct. In this region, due to large concentration gradients of the mass transfer species, the Sherwood numbers of the facets were generally higher than the periodic, fully-developed values.

The performance of the corrugated duct was evaluated under certain constraints. It was found that under certain conditions, the transfer coefficients of the corrugated duct are actually less than those of the corresponding straight duct.

REFERENCES

1. L. Goldstein, Jr. and E. M. Sparrow, Heat/mass transfer characteristics for flow in a corrugated wall channel, *Trans. Am. Soc. mech. Engrs*, Series C, *J. Heat Transfer* **99,** 187–195 (1977).
2. L. Goldstein, Jr. and E. M. Sparrow, Experiments on the transfer characteristics of a corrugated fin and tube heat exchanger configuration, *Trans. Am. Soc. mech. Engrs*, Series C, *J. Heat Transfer* **98,** 26–34 (1976).
3. J. E. O'Brien and E. M. Sparrow, Corrugated-duct heat transfer, pressure drop, and flow visualization, *Trans. Am. Soc. mech. Engrs*, Series C, *J. Heat Transfer* **104,** 410–416 (1982).
4. E. M. Sparrow and J. W. Comb, Effect of interwall spacing and fluid flow inlet conditions on a corrugated-wall heat exchanger, *Int. J. Heat Mass Transfer* **26,** 993–1005 (1983).
5. H. H. Sogin, Sublimation from disks to air streams flowing normal to their surfaces, *Trans. Am. Soc. mech. Engrs* **89,** 61–69 (1958).
6. B. V. Karlekar and R. M. Desmond, *Engineering Heat Transfer*, 2nd edn, p. 497. West, St. Paul, MN (1982).
7. V. Gnielinski, New equations for heat and mass transfer in turbulent pipe and channel flow, *Int. Chem. Engng* **16,** 359–386 (1976).
8. N. Cur and E. M. Sparrow, Turbulent heat transfer in a symmetrically or asymmetrically heated flat rectangular duct with flow separation at inlet, *Trans. Am. Soc. mech. Engrs, Series C, J. Heat Transfer* **104,** 82–89 (1982).
9. A. F. Mills, Experimental investigation of turbulent heat transfer in the entrance region of a circular conduit, *J. Mech. Engng* **4,** 63–77 (1962).
10. K. M. Krall and E. M. Sparrow, Turbulent heat transfer in the separated, reattached, and redevelopment regions of a circular tube, *Trans. Am. Soc. mech. Engrs*, Series C, *J. Heat Transfer* **88,** 131–136 (1966).
11. H. H. Sogin, A summary of experiments on local heat transfer from the rear or bluff obstacles to a low speed airstream, *J. Heat Transfer* **86,** 200–202 (1964).
12. V. G. Beloborodov and B. P. Volgin, Heat transfer and pressure drop in heat transfer equipment with slot channels of varying cross section, *Int. chem. Engng* **11,** 229–233 (1971).
13. O. C. Jones, Jr., An improvement in the calculation of turbulent friction in rectangular ducts, *J. Fluids Engng* 173–180 (June 1976).

EFFET DE L'ECARTEMENT DES PAROIS SUR LE TRANSFERT THERMIQUE ET LA PERTE DE CHARGE DANS UN CANAL A PAROIS CORRUGUEES

Résumé—Des expériences permettent de déterminer la distribution axiale des coefficients de convection thermique par facette et par cycle de l'écoulement turbulent dans un canal isotherme à parois corruguées avec différents écartements. L'étude est conduite à l'aide d'une technique de transfert massique. On considère deux régions du canal: la région d'entrée thermique et hydraulique et la région pleinement établie. Une technique de visualisation est utilisée pour examiner l'effet de l'écartement des parois sur la configuration de l'écoulement. Les résultats de perte de charge et de transfert thermique sont exploités pour évaluer les performances thermiques du canal.

EINFLUSS DES WANDABSTANDES AUF DEN WÄRMEÜBERGANG UND DEN DRUCKVERLUST IN EINEM KANAL MIT GEWELLTEN WÄNDEN

Zusammenfassung—Die axiale Verteilung der Wärmeübergangskoeffizienten bei turbulenter Strömung in einem Kanal mit isothermen gewellten Wänden wurde abhängig vom Wandabstand experimentell untersucht. Die Untersuchung wurde mit einem Stoffübergangs-Verfahren durchgeführt. Der Schwerpunkt der Studie lag auf zwei Gebieten des Kanals: thermisch–hydraulisches Eintrittsgebiet und das periodisch vollausgebildete Gebiet. Der Einfluß des Wandabstandes auf die Strömungsform wurde mit Hilfe eines besonderen Verfahrens zur Sichtbarmachung der Strömung untersucht. Die Ergebnisse über Druckverlust und Wärmeübergang wurden dazu verwendet, die thermische Leistungsfähigkeit des Kanals zu ermitteln.

ВЛИЯНИЕ РАЗМЕРНОГО ПАРАМЕТРА НА ТЕПЛООБМЕН И ПЕРЕПАД ДАВЛЕНИЯ В КАНАЛЕ С ГОФРИРОВАННЫМИ СТЕНКАМИ

Аннотация—Проведены эксперименты по определению осевого распределения значений коэффициентов теплообмена, приходящихся на каждую вогнутость и выпуклость для турбулентного течения в канале с гофрированными стенками и различным расстоянием между ними. Исследование проводилось методом измерения потока массы. Изучались две области канала: термогидродинамический входной участок и периодически повторяющаяся область развитого течения. При исследовании влияния расстояния между стенками на режим течения жидкости применялся метод визуализации. Полученные результаты по теплообмену и перепаду давления использованы для оценки тепловых характеристик канала.